European Journal of Neuroscience, Vol. 19, pp. 1257–1266, 2004

Effects of variability in anatomical reconstruction techniques on models of synaptic integration by dendrites: a comparison of three internet archives

Tibor Szilágyi[1,2] and Erik De Schutter[2]
[1]Department of Physiology, University of Medicine and Pharmacy, Str. Marinescu 38, 540139 Tg. Mures, Romania
[2]Laboratory of Theoretical Neurobiology, University of Antwerp, Belgium

Keywords: dendritic function, hippocampus, multicompartmental model, pyramidal neuron, rat

Abstract

The first step in building a realistic computational neuron model is to produce a passive electrical skeleton on to which active conductances can be grafted. For this, anatomically accurate morphological reconstructions of the desired cell type are required. In this study compartmental models were used to compare from a functional perspective three on-line archives of rat hippocampal CA1 pyramidal cell morphologies. The topological organization of cells was found to be similar for all archives, but several morphometric differences were observed. The three-dimensional size of the cells, the diameter and tortuosity of dendrites, and the electrotonic length of the main apical dendrite and of the branches in stratum lacunosum moleculare were dissimilar. The experimentally measured kinetics of somatically recorded inhibitory postsynaptic currents evoked in the stratum lacunosum moleculare (data from the literature) could be reproduced only using the archives that contained cells with an electrotonically short main apical dendrite. In the amplitude attenuation of the simulated postsynaptic currents and the voltage escape from the command potential under voltage clamp conditions, a two- to three-fold difference was observed among archives. Upon activation of a single model synapse on distal branches, cells with low dendritic diameter showed a voltage escape larger than 15 mV. The diameter of the dendrites influenced greatly the results, emphasizing the importance of methods that allow an accurate measurement of this parameter. Our results indicate that there are functionally significant differences in the morphometric data available in different archives even if the cell type, brain region and species are the same.

Introduction

A primary function of dendrites is the integration of synaptic inputs, which, depending on their location, produce somatic postsynaptic potentials with highly variable spatial and temporal patterns. Most neuron types possess a very diverse, intricately branched dendritic tree. Neurons can be classified according to their input/output relations with the rest of the neural network, and according to their morphology, for example differences in dendritic tree structure. Several modelling studies have been performed in order to understand the functional importance of these structural differences (e.g. hippocampal CA1 and CA3 pyramidal neurons and granule cells of the dentate gyrus (Carnevale *et al*., 1997); the same cell types complemented with interneurons (Cannon *et al*., 1999); calbindin-, calretinin- and parvalbumin-containing interneurons from hippocampal CA1 area (Emri *et al*., 2001)). All laboratories are using recording and staining techniques and histological protocols optimized for the scientific question under investigation. The methodological differences, however, can generate differences in the morphometric data with possible consequences on the simulated physiological behaviour of the cells. Whereas several studies have compared different neuron types, the differences attributable to the recording and reconstruction techniques used have been less explored. Most neuron models are built on a single dataset and interlaboratory differences are not taken into account. The morphology and passive membrane properties of a neuron underlie the interaction between the voltage-dependent currents and synaptic potentials (Rall, 1977). If differences are already present at the level of passive function of models, it is likely that more complex behaviour would also be affected.

With the recent publication of several dendritic morphologies, which are accessible through the Internet (Cannon *et al*., 1998; Megias *et al*., 2001), it is now possible to reconsider the importance of different electrical and morphological parameters affecting the cable properties of hippocampal CA1 pyramidal cells. In addition, dual intracellular recording with subsequent anatomical identification of the cells and synaptic contacts has provided knowledge regarding synaptic currents elicited in restricted domains of the dendritic tree (Buhl *et al*., 1994a). We combined this information and constructed models based on cell descriptions from three sources (Mainen *et al*., 1996; Pyapali *et al*., 1998; Megias *et al*., 2001). We statistically compared the morphometric parameters and assessed the alteration of synaptic currents originating from different domains of the dendritic tree, comparing them with inhibitory postsynaptic currents (IPSCs) obtained in a somatic voltage-clamp recording (Maccaferri *et al*., 2000). We estimate the effect of differences in morphological data and also evaluate errors associated with imperfect space-clamp.

Correspondence: Dr T. Szilágyi, [1]Department of Physiology, as above.
E-mail: tibor@bbf.uia.ac.be

Received 17 September 2003, revised 26 November 2003, accepted 17 December 2003

doi:10.1111/j.1460-9568.2004.03222.x

Materials and methods

Morphological data

Three-dimensional morphometric data describing rat hippocampal CA1 pyramidal cells were obtained from the following sources:

1. Duke/Southampton Archive of Neuronal Morphology (http://www.neuro.soton.ac.uk/). This archive contains *in vivo* and *in vitro* recorded cells, which were treated as separate groups in this study and are further referenced to as S_vivo ($n = 23$) and S_vitro ($n = 9$). Cells in both groups are from young animals; there exists a category of cells classified as originating from 'aged' animals that was not used here. Detailed description of these cells and information concerning the recording and reconstruction methods can be found in Pyapali *et al*. (1998).

2. The University of Texas at San Antonio, Laboratory of Dr Brenda Claiborne (http://www.utsa.edu/claibornelab/). This group is referenced to as UTSA ($n = 5$). Detailed information concerning these cells can be found in Mainen *et al*. (1996).

3. Institute of Experimental Medicine, Hungarian Academy of Sciences (http://www.koki.hu/~gulyas/ca1cells/cellfiles.htm). These cells were fully reconstructed by light microscopy and dendrites were classified into different subclasses in each layer, based on their order, spine density and distance from the soma. In a second step, samples of each dendritic subclass were re-embedded, serially sectioned and reconstructed by electron microscopy. This group will be referred to as HAS ($n = 17$). The cells and methods were presented in Megias *et al*. (2001).

Electrophysiological data

Maccaferri *et al*. (2000) recorded IPSCs evoked by four types of identified interneurons located in str. oriens. We used only their results from axo-axonic (Somogyi *et al*., 1983) and oriens-lacunosum moleculare (O-LM) cells, because these cells give synaptic terminals on highly restricted domains of the target pyramidal cells (axo-axonic cells on axon initial segments and O-LM cells in str. LM). Electrophysiological data for Fig. 6B were provided by G. Maccaferri and P. Somogyi.

Morphometric measurements and simulations

Passive models were constructed using the GENESIS (GEneral NEural SImulation System) simulation environment (Bower & Beeman, 1998). The three-dimensional (3-D) morphometric data were converted to GENESIS format by the CVAPP software (Cannon *et al*., 1998; http://www.compneuro.org) and by an in-house program written in Pascal/Delphi. This latter program was also used to measure all morphometric parameters. We used the Hines algorithm (Hines, 1984) available in GENESIS and the Crank–Nicolson implicit integration method with 5 μs time step. In order to increase computing efficacy, short, unbranched dendritic segments with identical diameter were collapsed into longer segments. The resulting compartment length was always below 0.05λ, where λ is the space constant. All reconstructions were inspected carefully, zero length segments were eliminated, and cells without filled branches in str. LM and those with ambiguous connectivity were not used for simulations. The thickness of dendrites in the UTSA database is overestimated, and therefore according to a thorough study using these cells (Mainen *et al*., 1996), the dendritic diameters were reduced by 0.5 μm for all compartments of cells in this group. The soma was represented as a 12-μm-diameter spherical compartment for the HAS and UTSA groups, and the lines specifying the soma contour were removed from the cell descriptor file. For cells from the S_vitro and S_vivo groups the original stack-like soma description was preserved but, for consistency, the total dendritic length, morphotonic length, surface area and volume were measured without the compartments marked as soma in the original database. In the original data for the HAS group the dendrites were already classified based on their position in different layers, order, spine density and distance from the soma. For cells from all other groups we sorted the dendrites by inspection of the 3-D structure and the corresponding dendrograms into the following categories: oriens, main apical shaft, apical oblique and LM. The apical oblique dendrites and the tuft-like ramifications in str. LM could be differentiated on the basis of their branching pattern and trajectories confined to str. radiatum or str. LM, respectively.

The slope of the cells relative to the plane of the slice was measured by the elevation of the apical tree, which was calculated as the angle between the XY-plane and the line passing through the soma and the centre of mass of all apical endpoints.

Dendritic spines were not explicitly modelled. To compensate for the missing spines, additional membrane area was incorporated. Based on an electron microscopic study of spine shape and density in the CA1 region of the rat hippocampus (Harris *et al*., 1992), the average cumulative spine area was considered to be 2.85 μm^2 per μm dendrite length. This spine area was taken to be constant for the whole dendritic tree. In order to obtain an unbiased comparison of cell groups, all cells were modelled with this spine compensation method, although for the HAS cells the spine density was available for each dendrite category. To investigate the effect of the more realistic spine densities (see Fig. 10), separate simulations were run for the HAS cells, with membrane area calculated on the basis of dendrite diameter, measured spine density (Megias *et al*., 2001) and an average spine surface area of 0.83 μm^2 (Harris & Stevens, 1989; Harris *et al*., 1992), giving a 1.0–3.7-fold surface expansion for the different dendrite types.

The electrotonic structure of the cells was described by morphotonic length (l_m), which is independent of the membrane and cytoplasmic electrical parameters:

$$l_m = 2l/\sqrt{(d)},$$

where l is the length, d the diameter of dendritic segments. The electrotonic length (L) can be calculated by: $L = l_m^*(R_i/R_m)^{1/2}$. The passive electrical parameters were uniform throughout the cell, and were within the following ranges: specific membrane capacitance (C_m), 0.7–1 $\mu F/cm^2$; specific membrane resistivity (R_m), 30–150 $k\Omega \cdot cm^2$; axial resistivity (R_i), 70–200 $\Omega \cdot cm$.

In all simulations the membrane potential was expressed relative to a −70 mV holding potential. The voltage-clamp circuit was modelled explicitly. A-type GABAergic synaptic input was modelled as a dual exponential conductance change:

$$g_{syn}(t) = \frac{A g_{max}}{\tau_1 - \tau_2}(e^{-t/\tau_1} - e^{-t/\tau_2}),$$

where τ_1 and τ_2 are the time constants describing the rising and decaying phases, respectively, and A is a normalization constant chosen such that the synaptic conductance (g_{syn}) reaches a maximum value of g_{max} (Bower & Beeman, 1998). Experimentally, the 10–90% rise time of miniture IPSCs at 35 °C in rat dentate gyrus granule neurons was measured to be in the submillisecond range, 0.3 ms (De Koninck & Mody, 1994), and 0.7 ms (Williams *et al*., 1998). In our simulations the time constants were 0.4 ms for the rising phase and 11 ms for the decay phase. In Maccaferri's experiments the pyramidal neurons were voltage clamped at a holding potential of −70 mV. The electrode filling solution had high Cl^- concentration (104 mM), and therefore we estimated the reversal potential of the $GABA_A$ receptor-mediated current using the Nernst equation at −8 mV, 62 mV positive to the holding potential. Maximum synaptic conductance was set to

0.5 nS, representing approximately the activation of one synapse (Hajos *et al*., 2000). The model synapse was placed systematically on each dendritic compartment and the somatic clamp current, the local synaptic current and the membrane potential at the location of the synapse were recorded. Attenuation was expressed as the ratio of maximal local synaptic current over maximal somatic clamp current. The mean attenuation in a dendritic domain was assessed by surface-weighted average attenuation ($Atten_{aver}$):

$$Atten_{aver} = \frac{\sum_{i=1}^{n} S_i Atten_i}{\sum_{i=1}^{n} S_i},$$

where $Atten_i$ and S_i are the attenuation and surface of the ith compartment, respectively, and n is the total number of compartments in the given dendritic domain.

The voltage escape owing to the space clamp error was described by the maximal deviation of the membrane potential from the holding potential at the site of the synapse.

Unless otherwise stated, results are expressed as mean ± standard deviation. Statistical comparison of cell groups was made by the Kolmogorov–Smirnov test. All statistical evaluation of morphometric data was performed without adding the surface area of dendritic spines, or taking them into account in any way. Simulation results obtained from all dendritic segments were summarized as Gaussian kernel density estimates (Silverman, 1986). This representation of relative frequencies captures better the continuous nature of the data, and contrary to histograms is not dependent on the end points of bins. We used kernel bandwidths of 5 or 10% of the data's overall standard deviation. The kernel's amplitude was normalized according to the surface of each compartment.

Results

Topologic comparison

The general structure of cells from all groups was similar (Fig. 1). No significant differences were observed in the number of branch points and endpoints, or maximum and average order of apical segments (Table 1). The maximum and average order of basal dendrites appeared significantly larger for S_vivo and S_vitro cells, but this difference was at least partially due to the fact that for these cells the soma was more accurately represented (as in the original database) by a stack of thin discs with the basal dendrites emerging from this stem, and not directly from the compartment arbitrarily designated as the root of the tree. Accordingly, for cells from the S_vivo and S_vitro groups, the total number of dendritic branch points was equal to the total number of endpoints minus 2. No other morphometric or electrical parameter was affected by this difference in the soma representation. Although the topological organization was similar, at quantitative morphometric level marked differences could be observed.

Morphometric comparison

The results of the morphometric measurements are summarized in Table 1. The total length of dendrites was larger for cells from the S_vitro and S_vivo groups than from the other two groups. The difference, however, reached statistical significance only in the S_vivo vs. HAS relation. The data points were scattered for the S_vivo and S_vitro groups, which could explain the lack of significance in the other comparisons (coefficient of variation (standard deviation/mean) of the total dendritic length was: S_vivo = 0.33, S_vitro = 0.29, UTSA = 0.13, HAS = 0.18). If the size of the cells was expressed as the distance of dendritic tips from the soma, measured along the dendrites, significant differences could be observed between the S_vitro or S_vivo group vs. UTSA or HAS group (Fig. 2). The difference was significant for both apical and basal dendrites. S_vitro vs. S_vivo as well UTSA vs. HAS groups did not differ significantly.

The average dendritic diameter was computed in two ways. If measured by the ratio between the total dendritic surface and total dendritic length, it was significantly larger for the UTSA group, and significantly smaller for the HAS group (Fig. 2). If the average diameter was assessed by the ratio between total volume and total surface, only the UTSA group, which had thicker dendrites, was significantly different from the others.

The total dendritic volume and surface area reflects the differences in both diameter and length. The cells with longer dendrites from the S_vitro and S_vivo groups had, however, a smaller volume and surface area than cells from the UTSA group, suggesting a dominant effect of the dendritic diameters. Cells from the HAS group, with the shortest

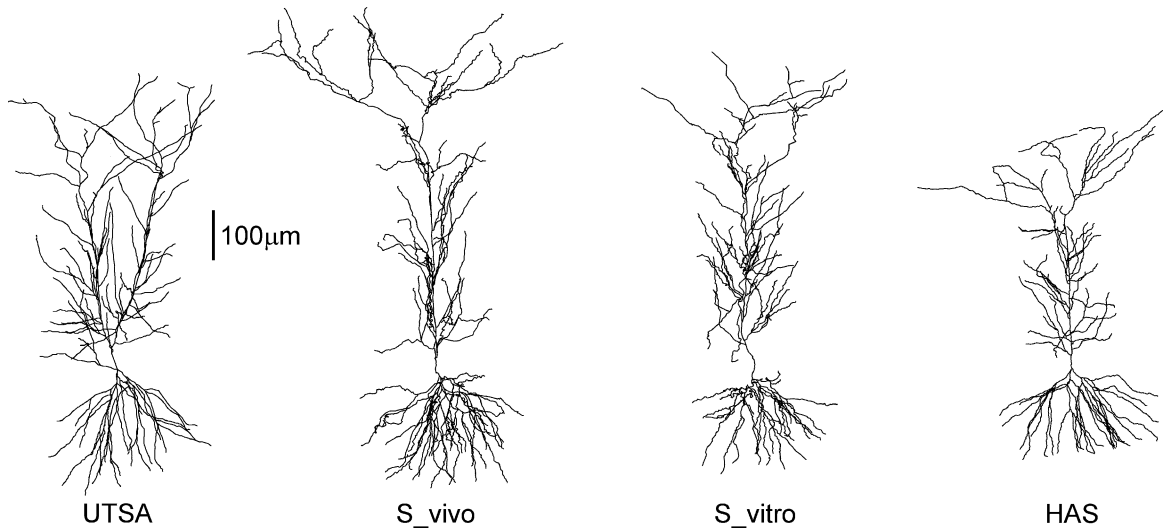

FIG. 1. Example cells from each group. The size in the x–y plane of the apical and basal dendritic tree of the displayed cells was within the mean ± 1 standard deviation boundaries of the group. The presented cell from the UTSA group had a bifurcated apical dendrite, but cells with this feature were also found in the other archives. The original names of the individual cells are: UTSA, 6028801; S_vivo, n407; S_vitro, n128; HAS, pc2b.

TABLE 1. Summary of morphometric data of CA1 pyramidal cells provided by different Internet databases

	UTSA	S_vivo	S_vitro	HAS	Statistical comparisons† a	b	c	d	e	f
Number of cells	5	23	9	17						
$MaxOrder_{Apical}$	26.60 ± 2.41	23.78 ± 6.14	25.00 ± 6.38	25.18 ± 4.46	–	–	–	–	–	–
$AverOrder_{Apical}$	14.65 ± 1.04	14.06 ± 2.82	14.65 ± 3.19	14.88 ± 2.25	–	–	–	–	–	–
$MaxOrder_{Basal}$	7.60 ± 1.34	10.57 ± 1.67	10.30 ± 2.31	8.06 ± 0.85	*	*	–	–	**	*
$AverOrder_{Basal}$	5.95 ± 0.86	7.66 ± 0.86	7.47 ± 1.01	6.34 ± 0.28	*	*	–	–	**	*
N_{Bp}	80.6 ± 11.8	84.3 ± 21.0	90.6 ± 26.8	75.1 ± 14.0	–	–	–	–	–	–
N_{Ep}	84.2 ± 12.2	86.3 ± 21.0	92.6 ± 26.8	78.9 ± 14.4	–	–	–	–	–	–
V (μm^3)	15093 ± 3749	21.04372	6377 ± 4030	4066 ± 586	*	*	**	–	*	–
S (μm^2)	47460 ± 8929	30647 ± 18630	29941 ± 11672	17425 ± 2936	*	–	**	–	**	*
L (μm)	12805 ± 1650	17705 ± 5914	15649 ± 4576	11668 ± 2136	–	–	–	–	**	–
L_m ($cm^{1/2}$)	240.8 ± 27.0	565.1 ± 190.7	455.6 ± 206.0	384.0 ± 74.3	*	*	*	*	**	–
V/S	0.315 ± 0.029	0.196 ± 0.062	0.200 ± 0.059	0.175 ± 0.016	*	*	**	–	–	–
S/L	3.691 ± 0.347	1.695 ± 0.698	1.940 ± 0.614	1.459 ± 0.093	*	*	**	–	*	*
$AverZ_{Ep}$ (μm)	47.2 ± 12.7	96.8 ± 68.4	53.0 ± 27.0	78.2 ± 16.5	–	–	*	–	–	*
$MaxD_{P,Apical}$ (μm)	822 ± 132	1354 ± 472	1144 ± 131	831 ± 53	*	*	–	–	**	**
$MaxD_{S,\ Apical}$ (μm)	656 ± 71	739 ± 158	642 ± 154	610 ± 56	–	–	–	*	**	–
$AverD_{P,\ Apical}$ (μm)	436 ± 80	648 ± 202	587 ± 89	408 ± 54	*	*	–	–	**	**
$AverD_{S,\ Apical}$ (μm)	350 ± 58	381 ± 103	317 ± 50	305 ± 33	–	–	–	–	*	–
$Tortuosity_{Apical}$	1.24 ± 0.09	1.70 ± 0.26	1.87 ± 0.24	1.34 ± 0.07	**	*	–	*	**	**
$MaxD_{P,\ Basal}$ (μm)	325 ± 39	553 ± 196	518 ± 70	303 ± 46	*	*	–	–	**	**
$MaxD_{S,\ Basal}$ (μm)	271 ± 31	301 ± 90	241 ± 56	250 ± 35	–	–	–	–	–	–
$AverD_{P,\ Basal}$ (μm)	241 ± 24	343 ± 116	325 ± 57	226 ± 28	–	*	–	–	**	**
$AverD_{S,\ Basal}$ (μm)	206 ± 27	188 ± 51	145 ± 23	191 ± 22	–	*	–	*	*	**
$Tortuosity_{Basal}$	1.17 ± 0.04	1.81 ± 0.24	2.30 ± 0.61	1.18 ± 0.06	**	*	–	–	**	**

All measurements were performed on morphometric data converted to Genesis format. The four groups give rise to six pairs of groups. The symbols indicate the probability P that the two groups came from the same population. MaxOrder, maximal branch order; AverOrder, average branch order of terminals; N_{Bp},N_{ep}, total number of branch points and endpoints; V, S, L, total dendritic volume, surface and length; L_m,total dendritic morphotonic length; $AverZ_{Ep}$, average absolute depth of endpoints; $MaxD_P$, maximum terminal path distance from the soma; $MaxD_S$, maximum terminal straight line distance from the soma; $AverD_P$, average path distance of terminals; $AverD_S$, average straight line distance of terminals; Tortuosity, $AverD_P/AverD_S$. The results of the Kolmogorov–Smirnov test for each pair of groups is shown in the right column. †Comparisons: a, UTSA vs. S_vivo; b, UTSA vs. S_vitro; c, UTSA vs. HAS; d, S_vivo vs. S_vitro; e, S_vivo vs. HAS; f, S_vitro vs. HAS. Low P values indicate a significant difference in the distributions. $^{**}P < 0.001$; $^{*}P < 0.05$; –, $P > 0.05$.

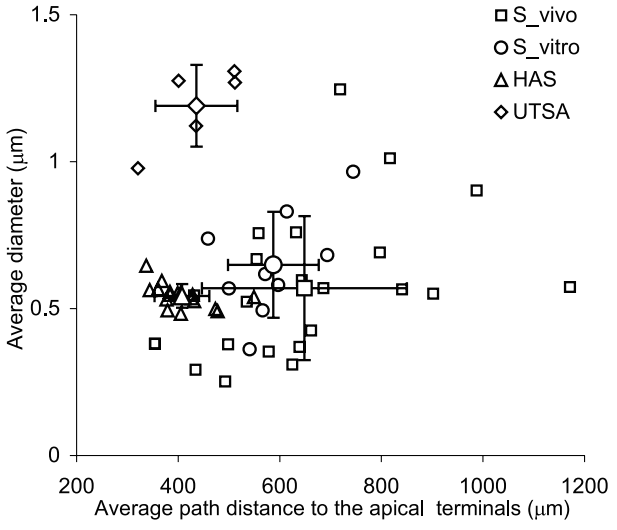

FIG. 2. Quantitative morphometric differences between cell groups. The size of cells (horizontal axis) is shown by the average distance from soma to all apical tips, measured along the branches. Average diameter (vertical axis) is expressed as $S_{tot}/(l_{tot}{}^{*}\pi)$, where S_{tot} is the total dendritic surface, and l_{tot} is the total length of apical branches. Each data point represents one cell. Cells from the S_vitro and S_vivo groups were significantly larger than cells from the other two sources. The average thickness of dendrites was significantly larger for the UTSA group than for the other groups.

and thinnest dendrites, had of course the smallest volume and surfacea area.

The total morphotonic length was shortest for the UTSA group, followed in order by the HAS, S_vitro and S_vivo groups. All groups were significantly different from each other, except HAS vs. S_vitro. However, the large variability of this parameter in the S_vitro group (coefficient of variation = 0.45) could obscure the difference.

The distance from soma to the dendritic tips was measured along the branches and in a straight line. The ratio of these two parameters indicates the deviation of dendrites from a straight line (Fig. 3). If there are no side ramifications, this parameter is a good measure for the sinuosity of dendrites. Therefore, it is more applicable to the radially spreading basal dendrites than to the apical tree, where the straight main apical shaft and the oblique ramifications always produce a relatively constant deviation from a straight line. Cells from the HAS and UTSA groups were similar and significantly less tortuous than cells from the S_vivo and S_vitro groups. On average, the basal dendrites of cells from the last group were more than twice as long when measured along the branches than the polar distance of dendritic endings, indicating a pronounced twisting of dendrites.

We next analysed the extent of the cells in the Z-direction by calculating the average of the absolute depth of all endpoints (Table 1). This parameter was larger for the *in vivo* labelled cells (S_vivo and HAS) then for the *in vitro* labelled cells (S_vitro and UTSA), but there was large scatter within the groups, so in most comparisons the difference was not significant. Measuring the elevation of the whole apical tree proved that there was a significant positive correlation ($P < 0.001$) between the extent of cells in the Z-direction and the slant of the cells (Fig. 4).

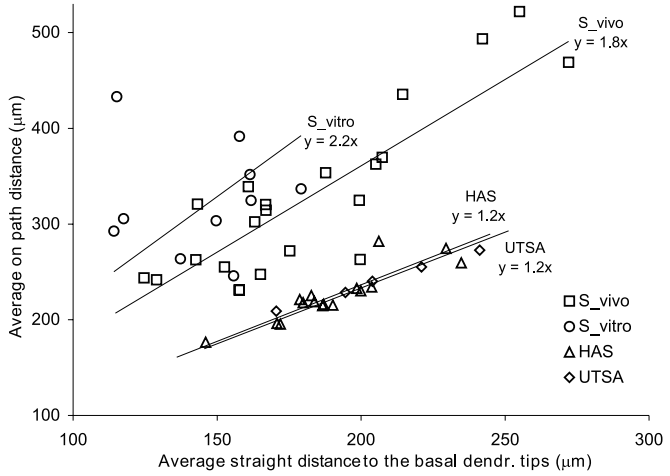

FIG. 3. Tortuosity of basal dendrites. The ratio of the distances from the soma to dendritic tips measured along the branches and in a straight line is a measure of tortuosity. A ratio of 1 would indicate a perfectly straight branch; higher values are indicative of deviation from linearity. The linear fits were forced to cross the origin of the coordinate system. Dendrites of cells from the S_vitro and S_vivo groups were found to be significantly more tortuous than those of cells from the other two sources.

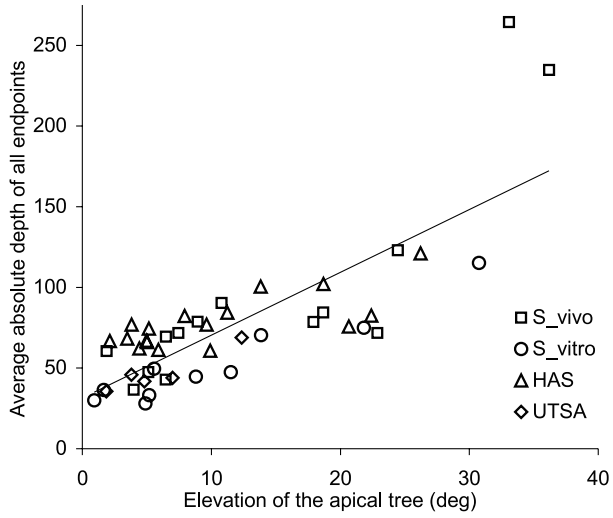

FIG. 4. Z-axis analysis of cell morphologies. The extent of the cells in the Z-direction was characterized by the average of the absolute depth of all endpoints. This was found to be significantly correlated to the elevation of the cells ($P < 0.001$).

Morphotonic comparison of dendrites in str. LM

The effects of morphological differences on the alteration of synaptic currents as they flow towards the soma were assessed first for synaptic inputs in str. lacunosum moleculare. This region is distant from the cell body layer and therefore the effects under investigation are expected to appear augmented.

Morphotonic analysis revealed that the main apical trunk reached str. LM at shorter morphotonic distance in the HAS and UTSA groups than in the S_vivo and S_vitro groups (Fig. 5). Meanwhile, owing to their larger diameter, dendrites of cells from the UTSA group travelled a shorter morphotonic distance in str. LM. As a result, this cell group was morphotonically the most compact. The average ratio of the morphotonic length from the entrance point into str. LM to the dendritic tips in this layer, and from the soma to the same dendritic tips, was $59.8 \pm 6.3\%$ for cells from the HAS group. This value was smaller for the other groups (UTSA, $40.0 \pm 3.3\%$; S_vitro, $43.9 \pm 6.9\%$; S_vivo, $52.2 \pm 7.0\%$). Some cells possessed bifurcated branches that entered str. LM with different diameters. In such cases, dendritic compartments located at the same anatomical distance could be at a different electrotonic length from the soma.

Comparison of synaptic events

Maccaferri *et al*. (2000) recorded IPSCs in CA1 pyramidal cells evoked by different types of anatomically identified interneurons located in str. oriens. The O-LM cells provide synaptic input to CA1 pyramidal neurons confined to str. lacunosum moleculare (Maccaferri *et al*., 2000). We tried to reproduce the time course of somatically recorded IPSCs elicited by these cells (10–90% rise time $= 6.2 \pm 0.6$ ms; mean $\pm$ SEM).

Simulations were run only on cells that had a clearly recognizable apical tuft ($n = 46$). In order to investigate which simulation parameters affect primarily the somatic IPSCs, and to assess what kind of variability could be expected from the experimental data, repeated simulations were run with a 100% change in different parameters (Fig. 6A). As expected from previous studies (Rinzel & Rall, 1974; Jack *et al*., 1975; Spruston *et al*., 1993), the most pronounced alteration of the IPSC was observed when the dendritic diameters or the axial resistivity were changed. Decreasing the membrane capacitance accelerated the IPSC but had less pronounced effect on its amplitude. Increasing the specific membrane resistivity, which makes the cell

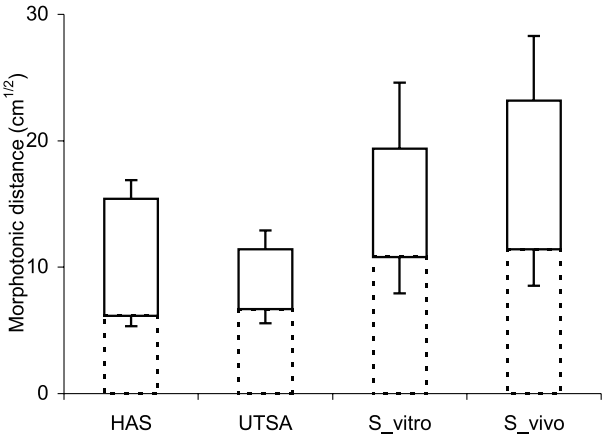

FIG. 5. Morphotonic length of dendrites in str. lacunosum moleculare. The lower bars (with dashed-line contour) represent the average morphotonic length of the main apical dendrite from soma to the entrance into str. LM. The upper, solid line bars denote the average morphotonic extent of dendrites in str. LM. Lower error bars indicate standard deviation of the morphotonic distance from soma to entry point(s) into str. LM. Upper error bars mark standard deviation of average morphotonic distance for all cells from a given group from soma up to the endpoints in str. LM. As branches in this layer are electrotonically the remotest from soma, the tops of columns denote the total morphotonic extent of cells in each group.

electrotonically more compact, caused a relatively small increase in the amplitude of somatic IPSC, and the kinetics became slower.

In Fig. 6B we show the electrophysiologically recorded IPSCs for comparison. The variability of the experimentally obtained 10–90% rise time was smaller than the effect of a 100% change in C_m, R_i or dendritic diameter (Fig. 6A). In contrast to the very small variability of 10–90% rise time, the decay phase was more variable.

Although we modelled synaptic conductance with a very fast rise time, using commonly accepted electrical parameters ($C_m = 1$ μF/cm^2,

$R_m = 30\,k\Omega\cdot cm^2$, $R_i = 200\,\Omega\cdot cm$) (Mainen *et al*., 1996; Carnevale *et al*., 1997; Cannon *et al*., 1999) all cell groups produced slower IPSCs than measured physiologically. Better fits were obtained with low cytoplasmic (axial) resistivity and low specific membrane capacitance (lowest values tested: $C_m = 0.7\,\mu F/cm^2$, $R_i = 70\,\Omega\cdot cm$). Increasing the specific membrane resistivity (tested range: 10–$150\,k\Omega\cdot cm^2$) slowed down the kinetics of IPSCs, an effect already pointed out by Spruston *et al*. (1993). With the above mentioned low values for C_m and R_i, activation of proximal LM synapses in cells with electrotonically short main apical trunk (HAS and UTSA) could reproduce the experimentally measured rise time (Fig. 7). Distal synapses were always too slow. Cells from the S_vitro and S_vivo groups could not reproduce the experimentally measured 10–90% rise time of IPSCs for any combination of electrical parameters within physiological range. Owing to the shorter electrotonic length of branches in str. LM, the variability of rise time was smaller for the UTSA group than for the other groups (narrower distribution on Fig. 7).

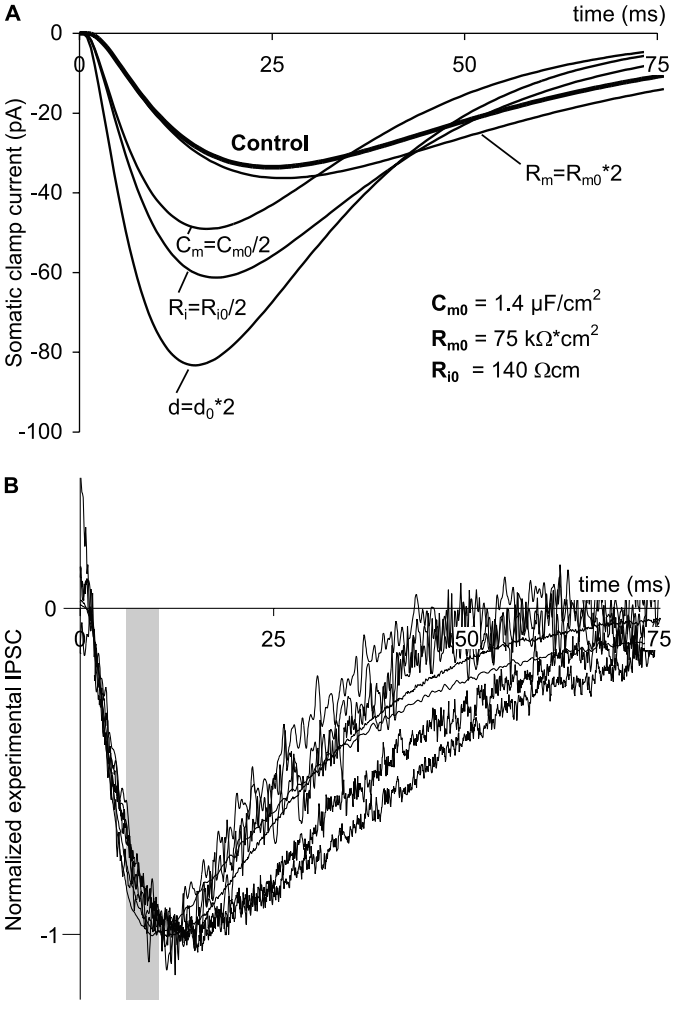

FIG. 6. Comparison of simulated (A) and experimentally recorded (B) IPSCs evoked in str. LM. Ten distal synapses were activated simultaneously in str. LM (A, cell pc1a from the HAS group). The parameters were doubled or halved in such a way as to increase the amplitude of the somatic IPSC. The modifications were evenly applied to all compartments. B displays the normalized average unitary IPSCs evoked by O-LM cells and recorded somatically from CA1 pyramidal cells by Maccaferri *et al*. (2000). The shaded area indicates the time interval, which comprises all experimentally measured 10–90% rise times. In contrast to the very small variability of 10–90% rise time, the decay phase was more variable. (Data for panel B courtesy of G. Maccaferri and P. Somogyi.)

The kinetics of IPSCs could have been attenuated and slowed down by current flowing in the distal direction at branch points. O-LM cells can provide 3–17 synaptic contacts on pyramidal cells (Maccaferri *et al*., 2000) and synchronous activation of these multiple distributed synaptic sites could prevent centrifugal current flow. We tested this hypothesis by modelling ten synapses distributed to cover all major dendritic branches in str. lacunosum moleculare. IPSCs obtained in this way were not faster, but actually were intermediate among traces obtained by activating the synapses individually (e.g. at cell n128 from the S_vitro group, for which the fastest synapse had a 10–90% rise time of 12.2 ms and the slowest 19.3 ms, activating all ten synapses synchronously resulted in a rise time of 15.5 ms).

Next we analysed the alteration of the synaptic current as it flows towards the soma and the local effect of the synaptic event. Our passive model predicts for str. LM synapses a surface-weighted average attenuation of IPSC amplitude in all cells: HAS = 3.8, UTSA = 3.3, S_vitro = 8.7 and S_vivo = 15.3 (Fig. 8A). IPSCs evoked in cells with an electrotonically longer main apical dendrite, from the S_vitro and S_vivo groups, suffered significantly more pronounced attenuation than cells from the other two groups.

Adequate space clamp was not possible for most of the synapses. In thin, distal dendrites (HAS, S_vitro and S_vivo groups) upon activation of a single synapse, the local membrane potential could deviate more than 15 mV from the holding potential (Fig. 8B). Cells from the UTSA group differed significantly from the other three groups, because none of the segments in str. LM presented more than 10 mV voltage escape. Beyond the main apical trunk, in less than 100 μm, the somatic voltage clamp reduced by less than 5% the dendritic inhibitory postsynaptic potential amplitude (perfect voltage clamp would be a 100% reduction).

After examining the effect of electrical parameters and dendritic diameter, the consequence of differences in 3-D structure and synapse location were investigated. Modelling the input systematically on all dendritic compartments, we could follow in details the dependence of the synaptic effect on the location of the synapse. As the synapse was

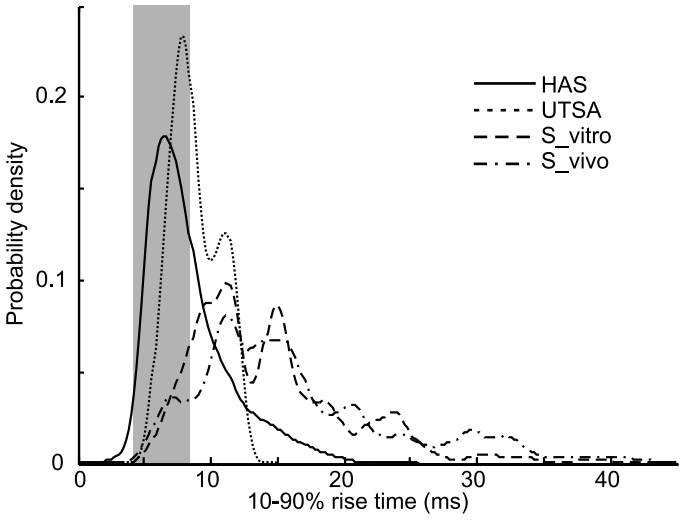

FIG. 7. Distribution of 10–90% rise time of IPSCs elicited in str. LM. The relative frequency distribution of all simulated segments is shown as a Gaussian kernel density estimate (see Methods). The shaded area indicates the time interval that comprises all experimentally measured values as in Fig. 6B. Cells in the HAS group had many segments that could reproduce the electrophysiological data. Cells from the UTSA group also had some pertinent segments, but cells from the S_vivo and S_vitro groups were barely compatible with these data. ($C_m = 0.7\,\mu F/cm^2$, $R_i = 70\,\Omega\cdot cm$, $R_m = 150\,k\Omega\cdot cm^2$, number of simulated segments: UTSA = 719, S_vivo = 1597, S_vitro = 640, HAS = 1944.)

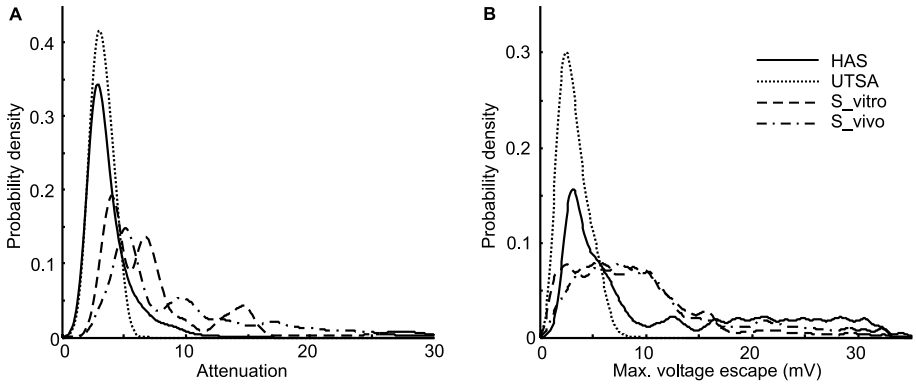

FIG. 8. Alteration of distal synaptic currents. Distribution of attenuation (A) and space clamp error (B) for all simulated segments in str. LM, shown as a Gaussian kernel density estimate. Attenuation is expressed as the ratio of maximal synaptic current and maximal somatic clamp current (abscissa truncated at 30). The space clamp error is indicated by the maximal voltage deviation from the holding potential at the site of the synapse. Contrary to attenuation and rise time, the space clamp error for HAS cells behaved differently from UTSA cells, as they had many segments with very large voltage deviation. Parameters as in Fig. 7.

moved distally along the frequently branching, thick main apical trunk, the rise time and attenuation of IPSCs increased progressively, whereas the voltage deviation from the holding potential changed only marginally (Fig. 9). When the synapse was placed on the thin terminal branches (apical obliques, distal LM and oriens) a pronounced voltage escape could be observed, but the rise time and attenuation was only slightly more increased than at the bifurcation point from where the branch originated. Owing to these factors, the morphological differences among the cell groups affected the IPSCs variably. Cells from the UTSA and HAS groups, having electrotonically short apical trunks, produced faster and less attenuated IPSCs than cells from the S_vivo or S_vitro groups. With regard to the space clamp error, however, the HAS cells, whose dendrites in str. LM were thin, behaved similarly to the S_vivo and S_vitro groups.

Finally, the effect of dendritic spines was investigated. Dendrites of cells from the HAS group had already been classified during the microscopic reconstruction into ten categories and the spine density was measured electron-microscopically for all ten dendrite types (Megias *et al*., 2001). Based on these data, we generated a new set of morphometric cell description files, incorporating spines using dendrite category-specific densities. Instead of the uniform 2.85 μm^2 per μm length, in this case the added membrane surface of dendrites ranged from 0.025 (the almost aspiny proximal apical shaft) to 5.8 μm^2 per μm length (distal part of the main apical trunk). Although this more realistic representation of spines improved the studied parameters of IPSCs, the effect was far less pronounced than the differences observed among cell groups (compare Fig. 10 with Figs 7 and 8)

Discussion

Clarifying the functional significance of the remarkable diversity in the structure of dendrites is essential for understanding how neurons and brain circuits work (Shepherd, 1998). Technological advances have made it possible to obtain complete and rather accurate morphometric descriptions of nerve cells, while computer power also became available to simulate anatomically detailed models. Building of neuronal morphology archives, which are available on the Internet, can make this information maximally accessible to interested researchers (Amari *et al*., 2002; Cannon *et al*., 2002; Gardner *et al*., 2003). The main finding of this paper is that there are significant differences in the morphometric data available in different archives, though the cell type, brain region and species are the same. It has been shown that these differences are functionally important: they alter the passive electrotonic properties of cells and modify the propagation of synaptic currents in the dendritic tree. Therefore, model neurons from different archives would have dissimilar integrative properties. We have avoided thorough theoretical analysis, but have focused more on practical implications for experimental investigators, who are using 'realistic' models to complement their electrophysiological observations.

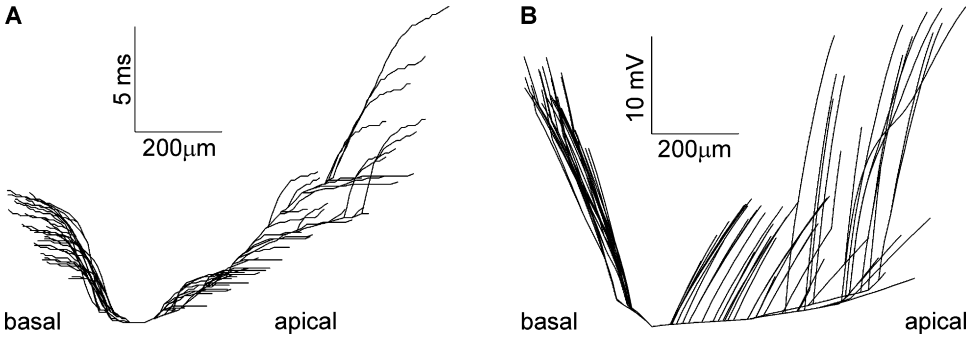

FIG. 9. Local and path-dependent factors shaping IPSCs. The 10–90% rise time of IPSCs (A) and space clamp error (B) is represented as a function of the anatomical distance of compartments from the soma (cell pc1a from the HAS group). The model synapse was placed in turn on all segments and a separate simulation was run for each compartment. Apical branches are drawn towards the right, whereas basal dendrites are drawn towards the left. The rise time slows as the activated synapse is further along the main branches and is relatively unaffected in the terminal branches. By contrast, the voltage deviation from the holding potential at the site of the synapse is minimal in the thick main branches and is steeply increasing as the synapse is positioned further along the thin terminal branches.

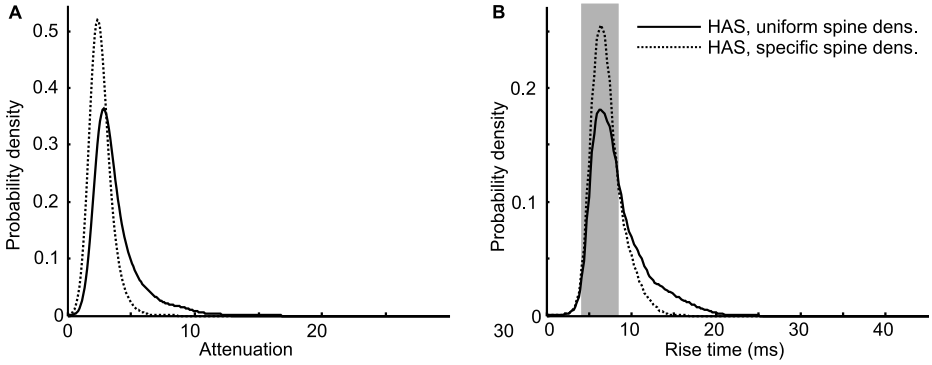

FIG. 10. Effect of dendritic spine density. Distribution of the attenuation (A) and 10–90% rise time (B) of IPSCs elicited in str. LM, shown as a Gaussian kernel density estimate. Solid lines represent the result of simulations of the HAS group with uniform spine density over all segments (as in Figs 7 and 8A). Dotted lines show the results from the same cells but with dendrites incorporating spines with segment type-specific densities. The shaded bar in B indicates the range of physiologically measured values as in Fig. 6B (number of simulated segments = 1944).

A recent study provides strong evidence that subtle differences in the dendritic structure of layer 5 neocortical pyramidal neurons may substantially influence their probability of coincidental detection (Schaefer *et al*., 2003). Another study has shown that differences in dendritic morphology of CA3 pyramidal cells can have a dramatic influence on the firing rate and firing mode (Krichmar *et al*., 2002). In spite of the fact that these studies demonstrate large variability of dendritic structure within the same class of neurons, the differences found between archives are more likely to arise from methodological differences.

All reconstructions were obtained from adult rats, but from different strains (UTSA, Sprague–Dawley; S_vitro, Fisher 344; S_vivo, Sprague–Dawley; HAS, Wistar). The recording and labelling techniques were also different, comprising *in vitro* and *in vivo* methods combined with intra- and extracellular labelling (for details see Claiborne *et al*., 1990; Mainen *et al*., 1996; Pyapali *et al*., 1998; Megias *et al*., 2001). Differences in the labelling methods, however, appear to be less important than dissimilarity in the histological processing techniques used. This is supported by the observation that cells from the S_vitro and S_vivo groups, which were recorded with quite different techniques, but processed in a similar way, were morphologically and electrotonically the most similar of the four groups analysed here. By contrast, the processing method greatly affects tissue shrinkage and the possibility of accurately measuring the diameter of dendrites. For the UTSA and HAS groups shrinkage correction was considered unnecessary, but for the S_vitro and S_vivo groups considerable shrinkage was measured by the authors, particularly in the depth of the sections (Pyapali *et al*., 1998), which was amended by applying a correction factor of 4.0 in this direction. The large shrinkage could explain the more wrinkled dendrites found in these groups compared with cells from the other two groups. Factors affecting the measurement of the dendritic diameter will be considered later, in a separate section.

Morphological differences

The topological organization of cells from all groups was similar, but the 3-D extent of the cells and the diameter of dendrites were dissimilar for neurons from different sources. The details are presented in Table 1. The most conspicuous differences were that cells from the S_vitro and S_vivo groups were larger, had electrotonically longer main apical dendrites and the dendrites were considerably more tortuous. Cells from the UTSA group were smaller, and their dendrites had larger diameter, which made them electrotonically the most compact group. Cells from the HAS group were anatomically the smallest, the main apical dendrite was electrotonically short (as in the UTSA group), but the branches in str. LM had small diameters; therefore their electrotonic length was large (as in the S_vitro and S_vivo groups).

The *in vivo* recorded cells (S_vivo and HAS) had a larger Z-extent than the *in vitro* recorded cells (S_vitro and UTSA). We found a significant positive correlation between Z-extent and the slant of the cells, suggesting that not the real size in depth but the cells' slope relative to the slice surface was different. Considering the difference in slice cutting procedures, this may explain the larger Z-extent of the *in vivo* filled cells.

Kinetics of IPSC

We tested to what extent the model neurons based on different reconstructions can reproduce the experimentally recorded IPSCs evoked by GABAergic interneurons in CA1 pyramidal cells (Maccaferri *et al*., 2000), and also assessed the degree to which morphological differences affect the passive electrophysiological behaviour of the models.

The decay time constant of synaptic events is less sensitive to dendritic filtering than the amplitude or rise time (Spruston *et al*., 1993) and, additionally, the available experimental data for the decay time constant were more scattered than data for the rise time (Fig. 6B); we therefore characterized the kinetics of simulated IPSCs only by their 10–90% rise time. The onset of the modelled synaptic conductance change was rapid (time constant of the rising phase 0.4 ms). The 10–90% rise time of IPSC evoked by a very proximal, perfectly clamped model synapse matched the experimental 10–90% rise time of axo-axonic cells (0.8 ± 0.1 ms; Maccaferri *et al*., 2000). This match suggests that the kinetic properties of the synaptic conductance change were chosen properly, because the axo-axonic cells innervate the CA1 pyramidal axon initial segments, which are very close to the soma, and the synaptic boutons are lined up in most cases on a single presynaptic axonal branch; therefore neither electrotonic filtering nor asynchrony in activation of synapses from different axonal branches can slow the time course of IPSCs (Li *et al*., 1992; Buhl *et al*., 1994b). Of course, it cannot be ruled out that distal synapses contain $GABA_A$ receptors with different subunit composition, which could confer them with unusually fast kinetics.

However, using the same synaptic conductance kinetics and commonly accepted electrical parameters ($C_m = 1\ \mu F/cm^2$, $R_m = 30\ k\Omega \cdot cm^2$, $R_i = 200\ \Omega \cdot cm$) none of the cell groups could reproduce the measured 10–90% rise time of IPSCs elicited by O-LM cells, which target distal dendritic shafts and spines. All groups produced too slow IPSCs, indicating that these electrical parameters, together with the morphologies tested, are incompatible with the experimental results. Because

decreased C_m and R_i generated faster somatic IPSCs, a better fit was expected with low values of these parameters. In neocortical pyramidal neuron dendrites, the axial resistivity was estimated to be 70–100 Ω·cm (Stuart & Spruston, 1998). The membrane capacitance can also be smaller than 1 μF/cm^2; a thorough study on hippocampal CA3 pyramidal neurons estimated $C_m = 0.7$–0.8 μF/cm^2 (Major *et al*., 1994). Using the lower range of these values ($C_m = 0.7$ μF/cm^2, $R_i = 70$ Ω·cm) proximal LM synapses of cells from the HAS and UTSA groups could reproduce the experimental rise time. The best matching models were obtained with cells from the HAS group. Cells from the S_vitro and S_vivo groups produced too slow IPSCs even with these electrical parameters. It is improbable that active conductances influenced our results because during the experiments whose results we used in our simulations (Maccaferri *et al*., 2000), the cells were voltage-clamped at −70 mV using electrodes containing CsCl and QX-314. We can assume that under these conditions, most voltage-dependent ion channels, active around resting membrane potential, were closed.

The dendritic architecture affects the passive normalization of synaptic inputs (Jaffe & Carnevale, 1999). Neocortical and CA1 neurons, which possess a long apical dendrite, show substantial location-dependent variability of somatic postsynaptic potentials (small normalization); by contrast, in cells that lack long primary dendrites less location dependency is observed. The electrotonic length of the main apical dendrite of these cells is therefore an important factor shaping the amplitude and time course of somatic IPSCs. Indeed, the electrotonically short main apical trunk was a common property of cells from the HAS and UTSA groups, which were compatible with the electrophysiological data.

Dendritic branches spanned a very long electrotonic distance in str. LM, and therefore the morphological information alone, that a synapse is situated in str. LM, is a poor indicator of its electrotonic distance from the soma. In addition, when cells possessed a bifurcated main apical dendrite, which entered str. LM with different diameters, even synapses located at the same anatomical distance from the soma generated synaptic currents with very different kinetics.

Effect of dendritic spines on IPSCs

For the HAS cell group we tested the effect of modifying the density of dendritic spines. When the morphometric data with uniform spine density were replaced by more realistic cell descriptions with dendrite-type specific spine density (Megias *et al*., 2001), the parameters of simulated IPSCs improved. The change was, however, less prominent than the differences between archives.

Attenuation of IPSCs

The attenuation of somatically recorded IPSCs shows characteristic differences between cell groups. The IPSCs originating from str. LM, were on average less attenuated in cells from the HAS and UTSA groups than in cells from the S_vivo and S_vitro groups. Synaptic current flowing centripetally, i.e. towards the soma, is more attenuated along the main apical dendrite than in the terminal branches (Carnevale *et al*., 1997), and therefore cells from the HAS group, although possessing electrotonically long dendrites in str. LM, had a similar attenuation to those of the UTSA group.

Space-clamp error

Except at the main apical trunk, the dendritic membrane potential was very poorly controlled by the somatic voltage clamp, which hardly reduced the local amplitude of the inhibitory postsynaptic potentials. Whereas in the proximal branches the local membrane potential change was just a few millivolts, in distal branches the deviation from the command potential was greater than 15 mV. The voltage escape abruptly increased in the terminal dendritic branches, and was very sensitive to the dendritic diameters, explaining the significantly smaller escape in the UTSA cells. This can partially account for the relatively small escape found in a study using these cells (Jaffe & Carnevale, 1999). Excitatory synaptic conductance transients decay faster than the inhibitory postsynaptic currents used here, which could also contribute to the reduced voltage escape. Our results indicate that in experiments using a somatic voltage-clamp it is virtually impossible to control precisely the membrane potential beyond the main apical trunk. In spite of the fact that basal dendrites are anatomically closer to the soma, they experience a space clamp error similar to the apical dendrites, because the voltage escape is mainly increasing in the thin terminal branches, and not along the main apical dendrite. Our study, by using real morphologies and a more complex compartmental model, complements and extends the results of Spruston *et al*. (1993).

Effect of dendritic diameters on IPSCs

The diameter of dendrites can alter the effectiveness of a synapse (Holmes, 1989; Wolf *et al*., 1992). In our simulations the diameter of dendrites and the cytoplasmic resistivity had the largest effect on IPSCs elicited in str. LM. Both factors directly affect the axial current flow and their influence can partially explain that cells from the UTSA group had the smallest space clamp error and attenuation of IPSCs. Statistical comparison revealed significant difference in the average diameter of dendrites. Cells from the UTSA group had the largest diameters, HAS group the smallest, and S_vitro and S_vivo groups intermediate values. Unfortunately, the diameter of dendrites is the most difficult morphological parameter to determine. Permeabilization of membranes during histological processing (e.g. by Triton) might cause leakage of the peroxidase reaction product. The distortion of light microscopic methods makes it difficult to measure the diameter of small dendrites accurately, especially in thick slices (as with the UTSA group). Even if there was an optimal filling and processing method, the light microscopic reconstructions remain prone to human error (Jaeger, 2000). When neurons were reconstructed independently by two researchers, a recent study reports a 19% difference in electrical parameters estimated by fitting simulation results to electrophysiological data (Steuber *et al*., 2004). The accuracy of diameter measurements could be improved if critical segments were measured also by electron microscopy. This was performed for HAS cells, but in this case only the diameter of a limited number of samples was measured for each dendrite type. Diameters obtained in this way were extrapolated to all segments belonging to the same class.

Conclusions

Models with identical electrical parameters but built on morphometric data from different resources had significantly different functional properties. Therefore, it is recommended to test the robustness of any detailed neuron model against the variability of the morphometric data.

Inaccuracy in morphological measurement can be compensated by electrical parameters, e.g. dendritic diameter by cytoplasmic resistivity (Major, 2000). The significant differences in the morphometric data suggest that it is difficult to define at a quantitative level a universally valid CA1 pyramidal cell prototype. Therefore, it would be more important to fit the passive electrical parameters to the electrophysiological behaviour of the corresponding neuron (Major *et al*., 1994) than trying to find accurate absolute values. However, if only anatomical data are published in the Internet databases, this compensation cannot be performed. Therefore, for intracellularly recorded neurons, it would be useful to publish alongside morphological descriptions

electrophysiological data from the same cell, which could be used to constrain the electrical parameters.

Acknowledgements

We are grateful to all contributors and those maintaining the shared neuron databases, which provided high-quality neural reconstructions. We thank Péter Somogyi at MRC Anatomical Neuropharmacology Unit, Oxford, and Gianmaria Maccaferri at Northwestern University, Chicago, for providing the electrophysiological data. We thank Zsuzsa Emri and Reinoud Maex for their useful comments on the manuscript. This work was supported by BOF-UA (BWTS03), FWO (G.0401.00) and European Commission (QLRT-2000-01241) grants.

Abbreviations

3-D, three-dimensional; C_m, specific membrane capacitance; IPSC, inhibitory postsynaptic current; O-LM cell, oriens-lacunosum moleculare cell; R_i, axial (cytoplasmic) resistivity; R_m, specific membrane resistivity; str. LM, stratum lacunosum moleculare.

References

Amari, S.-I., Beltrame, F., Bjaalie, J.G., Dalkara, T., De Schutter, E., Egan, G.F., Goddard, N.H., Gonzalez, C., Grillner, S., Herz, A., Hoffmann, K.-P., Jaaskelainen, I.P., Koslow, S.H., Lee, S.-Y., Matthiessen, L., Miller, P.L., Da Silva, F.M., Novak, M., Ravindranath, V., Ritz, R., Ruotsalainen, U., Sebestra, V., Subramaniam, S., Tang, Y.Q., Toga, A.W., Usui, S., Pelt, J.V., Verschure, P., Willshaw, D. & Wrobel, A. (2002) Neuroinformatics: the integration of shared databases and tools towards integrative neuroscience. *J. Integrative Neurosci.*, **1**, 117–128.

Bower, J.M. & Beeman, D. (1998) *The Book of GENESIS – Exploring Realistic Neural Models with the General Neural Simulation System*. Springer – TELOS, New York.

Buhl, E.H., Halasy, K. & Somogyi, P. (1994a) Diverse sources of hippocampal unitary inhibitory postsynaptic potentials and the number of synaptic release sites. *Nature*, **368**, 823–828.

Buhl, E.H., Han, Z.-S., Lorinczi, Z., Stezhka, V.V., Karnup, S.V. & Somogyi, P. (1994b) Physiological properties of anatomically identified axo-axonic cells in the rat hippocampus. *J. Neurophysiol.*, **71**, 1289–1307.

Cannon, R.C., Howell, F.W., Goddard, N.H. & De Schutter, E. (2002) Non-curated distributed databases for experimental data and models in neuroscience. *Network: Computation Neural Systems*, **13**, 415–428.

Cannon, R.C., Turner, D.A., Pyapali, G.K. & Wheal, H.V. (1998) An on-line archive of reconstructed hippocampal neurons. *J. Neurosci. Meth.*, **84**, 49–54.

Cannon, R.C., Wheal, H.V. & Turner, D.A. (1999) Dendrites of classes of hippocampal neurons differ in structural complexity and branching patterns. *J. Comp. Neurol.*, **413**, 619–633.

Carnevale, N.T., Tsai, K.Y., Claiborne, B.J. & Brown, T.H. (1997) Comparative electrotonic analysis of three classes of rat hippocampal neurons. *J. Neurophysiol.*, **78**, 703–720.

Claiborne, B.J., Amaral, D.G. & Cowan, W.M. (1990) Quantitative, three-dimensional analysis of granule cell dendrites in the rat dentate gyrus. *J. Comp. Neurol.*, **302**, 206–219.

De Koninck, Y. & Mody, I. (1994) Noise analysis of miniature IPSCs in adult rat brain slices: properties and modulation of synaptic GABAA receptor channels. *J. Neurophysiol.*, **71**, 1318–1335.

Emri, Z., Antal, K., Gulyas, A.I., Megias, M. & Freund, T.F. (2001) Electrotonic profile and passive propagation of synaptic potentials in three subpopulations of hippocampal CA1 interneurons. *Neuroscience*, **104**, 1013–1026.

Gardner, D., Toga, A.W., Ascoli, G.A., Beatty, J.T., Brinkley, J.F. & Dale, A.M. (2003) Towards effective and rewarding data sharing. *Neuroinformatics*, **1**, 289–296.

Hajos, N., Nusser, Z., Rancz, E.A., Freund, T.F. & Mody, I. (2000) Cell type- and synapse-specific variability in synaptic GABAA receptor occupancy. *Eur. J. Neurosci.*, **12**, 810–818.

Harris, K.M., Jensen, F.E. & Tsao, B. (1992) Three-dimensional structure of dendritic spines and synapses in rat hippocampus (CA1) at postnatal day 15 and adult ages: implications for the maturation of synaptic physiology and long-term potentiation. *J. Neurosci.*, **12**, 2685–2705.

Harris, K.M. & Stevens, J.K. (1989) Dendritic spines of CA 1 pyramidal cells in the rat hippocampus: serial electron microscopy with reference to their biophysical characteristics. *J. Neurosci.*, **9**, 2982–2997.

Hines, M. (1984) Efficient computation of branched nerve equations. *Int. J. Biomed. Comput.*, **15**, 69–76.

Holmes, W.R. (1989) The role of dendritic diameters in maximizing the effectiveness of synaptic inputs. *Brain Res.*, **478**, 127–137.

Jack, J.J.B., Noble, D. & Tsien, R.W. (1975) *Electric Current Flow in Excitable Cells*. Clarendon Press, Oxford.

Jaeger, D. (2000) Accurate reconstruction of neuronal morphology. In: De Schutter, E. (Ed.), *Computational Neuroscience: Realistic Modeling for Experimentalists*. CRC Press, Bota Racon, FL, pp. 159–178.

Jaffe, D.B. & Carnevale, N.T. (1999) Passive normalization of synaptic integration influenced by dendritic architecture. *J. Neurophysiol.*, **82**, 3268–3285.

Krichmar, J.L., Nasuto, S.J., Scorcioni, R., Washington, S.D. & Ascoli, G.A. (2002) Effects of dendritic morphology on CA3 pyramidal cell electrophysiology: a simulation study. *Brain Res.*, **941**, 11–28.

Li, X.-G., Somogyi, P., Tepper, J.M. & Buzsaki, G. (1992) Axonal and dendritic arborization of an intracellularly labeled chandelier cell in the CA1 region of rat hippocampus. *Exp. Brain Res.*, **90**, 519–525.

Maccaferri, G., Roberts, J.D., Szucs, P., Cottingham, C.A. & Somogyi, P. (2000) Cell surface domain specific postsynaptic currents evoked by identified GABAergic neurones in rat hippocampus in vitro. *J. Physiol. (Lond.)*, **524**, 91–116.

Mainen, Z.F., Carnevale, N.T., Zador, A.M., Claiborne, B.J. & Brown, T.H. (1996) Electrotonic architecture of hippocampal CA1 pyramidal neurons based on three-dimensional reconstructions. *J. Neurophysiol.*, **76**, 1904–1923.

Major, G. (2000) Passive cable modeling – a practical introduction. In: De Schutter, E. (Ed.), *Computational Neuroscience: Realistic Modeling for Experimentalists*. CRC Press, Bota Racon, FL, pp. 209–232.

Major, G., Larkman, A.U., Jonas, P., Sakmann, B. & Jack, J.J.B. (1994) Detailed passive cable models of whole-cell recorded CA3 pyramidal neurons in rat hippocampal slices. *J. Neurosci.*, **14**, 4613–4638.

Megias, M., Emri, Z., Freund, T.F. & Gulyas, A.I. (2001) Total number and distribution of inhibitory and excitatory synapses on hippocampal CA1 pyramidal cells. *Neuroscience*, **102**, 527–540.

Pyapali, G.K., Sik, A., Penttonen, M., Buzsaki, G. & Turner, D.A. (1998) Dendritic properties of hippocampal CA1 pyramidal neurons in the rat: intracellular staining in vivo and in vitro. *J. Comp. Neurol.*, **391**, 335–352.

Rall, W. (1977) Core conductor theory and cable properties of neurons. In: Kandel, E.R. (Ed.), *Handbook of Physiology. The Nervous System: Cell Biology of Neurons*. American Physiological Society, Bethesda, MD, pp. 39–97.

Rinzel, J. & Rall, W. (1974) Transient response in a dendritic neuron model for current injected at one branch. *Biophys. J.*, **14**, 759–790.

Schaefer, A.T., Larkum, M.E., Sakmann, B. & Roth, A. (2003) Coincidence detection in pyramidal neurons is tuned by their dendritic branching pattern. *J. Neurophysiol.*, **89**, 3143–3154.

Shepherd, G.M. (1998) *The Synaptic Organization of the Brain*. Oxford University Press, New York.

Silverman, B.W. (1986) *Density Estimation for Statistics and Data Analysis*. Chapman & Hall, London.

Somogyi, P., Nunzi, M.G., Gorio, A. & Smith, A.D. (1983) A new type of specific interneuron in the monkey hippocampus forming synapses exclusively with the axon initial segments of pyramidal cells. *Brain Res.*, **259**, 137–142.

Spruston, N., Jaffe, D.B., Williams, S.H. & Johnston, D. (1993) Voltage- and space-clamp errors associated with the measurement of electrotonically remote synaptic events. *J. Neurophysiol.*, **70**, 781–802.

Steuber, V., De Schutter, E. & Jaeger, D. (2004) Passive models of neurons in the deep cerebellar nuclei the effect of reconstruction errors. *Neurocomputing*, **59**, in press.

Stuart, G. & Spruston, N. (1998) Determinants of voltage attenuation in neocortical pyramidal neuron dendrites. *J. Neurosci.*, **18**, 3501–3510.

Williams, S.R., Buhl, E.H. & Mody, I. (1998) The dynamics of synchronized neurotransmitter release determined from compound spontaneous IPSCs in rat dentate granule neurones in vitro. *J. Physiol. (Lond.)*, **510**, 477–497.

Wolf, E., Birinyi, A. & Szekely, G. (1992) Simulation of the effect of synapses: the significance of the dendritic diameter in impulse propagation. *Eur. J. Neurosci.*, **4**, 1013–1021.